

# Multi-Scale Depth from Slope with Weights

BMVC 2010 Submission # 190

## Abstract

We describe a robust method to recover the depth coordinate from a normal or slope map of a scene, obtained e.g. through photometric stereo or interferometry. The key feature of our method is the fast solution of the Poisson-like integration equations by a multi-scale iterative technique. The method accepts a weight map that can be used to exclude regions where the slope information is missing or untrusted, and to allow the integration of height maps with linear discontinuities (such as along object silhouettes) which are not recorded in the slope maps. Except for pathological cases, the memory and time costs of our method are typically proportional to the number of pixels  $N$ . Tests show that our method is as accurate as the best weighted slope integrators, but substantially more efficient in time and space.

## 1 Introduction

The *integration of a slope map* to yield a height (or depth) map is a computational problem that arises in several computer vision contexts, such as shape-from-shading [11, 12] and multiple-light photometric stereo [13, 27]. This problem has many important real-world applications. See figure 1.

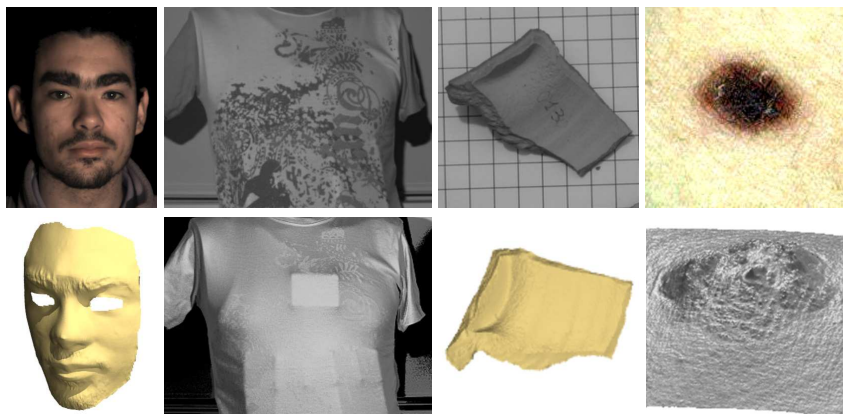


Figure 1: Some applications of slope integration in photometric stereo: 3D face capture [10], security inspections [24], archaeology [14, 20], and dermatology [23].

Abstractly, in this problem we want to determine an unknown real function  $Z$  defined on some region  $D$  of  $\mathbb{R}^2$ , given its gradient  $\nabla Z = (\partial Z/\partial x, \partial Z/\partial y)$ . That is, we wish to find  $Z$

such that  $\partial Z/\partial x = F$  and  $\partial Z/\partial y = G$ , where  $F$  and  $G$  are two given real functions defined on  $D$ . It is well known that this problem has a differentiable solution if and only if the field  $(F, G)$  is curl-free, that is  $\partial F/\partial y - \partial G/\partial x = 0$  everywhere. Then the function  $Z$  can be expressed as a line integral along any path from a reference point  $(x_0, y_0)$  to  $(x, y)$ .

In practical contexts, however, there are at least three difficulties with this approach. First, the slope functions  $F$  and  $G$  are generally *discretized*, i.e. known only at certain *slope sampling points*  $p[u, v]$ , which usually form a regular orthogonal grid. Second, the data is usually contaminated with *noise* arising from unavoidable measurement, quantization, and computation errors. At some points, the expected magnitude of the error may be so high that the slope is essentially unknown; and this may happen over large regions of the domain  $D$ . Third, the height function  $Z$  is usually *discontinuous*. The height field  $Z(x, y)$  of a real scene almost always has *cliffs*—step-like discontinuities along the silhouettes of solid objects. Some slope acquisition technologies, including most photometric stereo methods, will severely underestimate the mean slope across cliffs. Slope values will also be meaningless wherever the height itself is poorly defined, e.g. where the scene is highly porous, transparent, or covered with hair. In general, neither the position nor the magnitude of these anomalies can be deduced from the slope maps alone. Because of these complications, algorithms that may seem valid in theory (such as path integration) often yield very poor results when applied to real world data. Several integration methods that have been described in the literature (see section 2) are unsuitable for photometric stereo, either for being too sensitive to noise and cliffs, or for being too costly for use with high-resolution maps

In this paper we describe a multi-scale iterative integration procedure that is as accurate and robust as the best existing methods, but substantially more efficient. Except for some pathological cases, its memory and time cost scales linearly with the number of data pixels, making it quite practical even for multi-megapixel maps.

Like the best existing methods [3], our procedure also accepts a *weight map* that specifies the reliability of each gradient sample and the location of suspected cliff discontinuities. This information allows the procedure to ignore unreliable data and to avoid integrating the slope across cliffs. The weight map can be obtained in many ways, either from external information or as a result of error detection algorithms applied to the slope data [2, 3, 4, 5, 16, 18, 22]. Most of these weight acquisition techniques can be used with our integrator as well. In this paper, however, we are concerned only with the central integration problem, assuming that the slope and weight maps are given and fixed.

## 2 Related Work

Most of the previous algorithms for the integration of slope maps can be classified into four broad groups: *path integration*, *Fourier filtering*, *local iteration*, and *direct system solving*.

**Path-integration methods** assign a height to one reference pixel  $p$  and then compute the height of every other pixel  $q$  by performing a numerical line integral of the gradient field along a path from  $p$  to  $q$ . This group includes the naive row-by-row integration [28] as well as other methods that choose the paths so as to avoid low-quality or missing data—e.g. by finding an optimum spanning tree and integrating along it, as done by Fraile and Hancock [2, 7]. These methods are generally quite fast, since they require only  $O(N)$  operations for an image with  $N$  pixels. However, they are very sensitive to noise and discontinuities: if the heights of two adjacent pixels  $p', p''$  are computed by distinct paths, integration of the noise component of the gradient will result in a spurious height difference between them.

This problem can be alleviated, but not solved, by averaging the integral along many distinct paths between the two pixels [19]. While this approach gets rid of spurious steps due to noise, its cost is prohibitive (proportional to  $N^{2.5}$  for an image with  $N$  pixels) and its results are still inferior to those of non-path methods described below.

**Fourier filtering methods** are based on the observation that integrating a function corresponds to dividing each component of the Fourier transform by  $2\pi$  times its frequency. This approach was pioneered by Frankot and Chellapa [8]. In the Fourier domain the curl component of the gradient data can be easily filtered out, and other smoothing filters can be applied as well [26]. Fourier techniques can be used also to efficiently solve the unweighted Poisson equation (see below) as done by Georghiadis *et al.* [9].

Through the use of fast Fourier transform algorithms (FFT or DCT), these methods obtain the height field for  $N$  pixels using only  $O(N)$  space and  $O(N \log N)$  operations. However, this approach does not allow the use of a weight map, because the FFT always gives the same weight to all data samples. As a result, these methods will flatten out any invisible cliffs and deform the surface over a wide area surrounding them.

**Local iteration methods** reduce the slope integration problem to a system of  $N$  equations whose unknowns are the  $N$  heights, and where each equation relates one height value and its neighbors to the given derivatives in that neighborhood. The equations (whether linear or non-linear) are then solved as in the Gauss-Seidel iterative method: starting with some initial guess, each equation is solved in turn to recompute one height value, assuming the neighbors are fixed, until all the heights appear to stabilize [11, 17].

The local equations can be derived in several ways [3, 11, 21]. However, all these local criteria generally yield some discrete (and possibly non-linear) version of Poisson's equation  $\nabla^2 Z = h(x, y)$ . Since each equation refers to a small number of height values, the whole system uses only  $O(N)$  storage. This formulation does not generate spurious steps like the path-integration methods. Indeed, the solution is theoretically equal to that of the Fourier filtering. The advantage of the iterative formulation, as pointed out by Agrawal *et al.* in 2006 [3], is that each equation can be tuned to ignore bad data samples and suspected discontinuities, as indicated by a weight map. On the other hand, although each iteration requires only  $O(N)$  operations, the number of iterations needed to reduce the error below a specified tolerance is usually proportional to the square of the image's diameter, that is to  $N$ ; so the total running time is proportional to  $N^2$ .

In 2004, Chen, Wang and Wang described a "pyramid-based" method to speed up iterative solution of the Poisson equations [6]. Their method (which does not accept weights) solves a sequence of  $N \times N$  Poisson systems, where at stage  $k$  each height  $z[u, v]$  is related to heights  $z[u \pm 2^k, v \pm 2^k]$ . While the use of longer strides substantially improved the convergence of the iteration, the speed and accuracy of this method were still quite inferior to those of Fourier-based algorithms.

**Direct system solving methods** also set up an  $N \times N$  system of equations from local constraints, but solve the system by a direct method, such as Gaussian LU or Cholesky factorization. (If the equations are non-linear, they must be linearized and the process must be iterated over, as in the Newton-Raphson method.) This approach is used, in particular, by several of Agrawal's "Poisson based" methods. [3].

Direct solution methods are generally slower than Fourier methods but much faster than iterative ones. However, their running time grows like  $O(N^{1.5})$ , according our tests; and their memory requirements (even with good sparse matrix software) makes them impractical for multi-megapixel slope maps.

### 3 Weighted multiscale integration

Our multiscale integrator builds the linear equation system for a weighted variant of the discrete Poisson problem, and solves it by the Gauss-Seidel (or Gauss-Jacobi) iterative algorithm. Unlike other local iterative methods, it obtains the initial guess by recursively solving a reduced scale version of the problem. Namely, it reduces the given slope maps  $f, g, w$  to one half of their original width and height, recursively computes from them a reduced-scale height map  $z$ , expands the latter to twice its size, and uses the Gauss-Seidel iteration to adjust this map according to the full-scale slope data. The recursion stops at a level  $m$  where the slope maps are so small that the iteration will quickly converge from any initial guess. See figure 2.

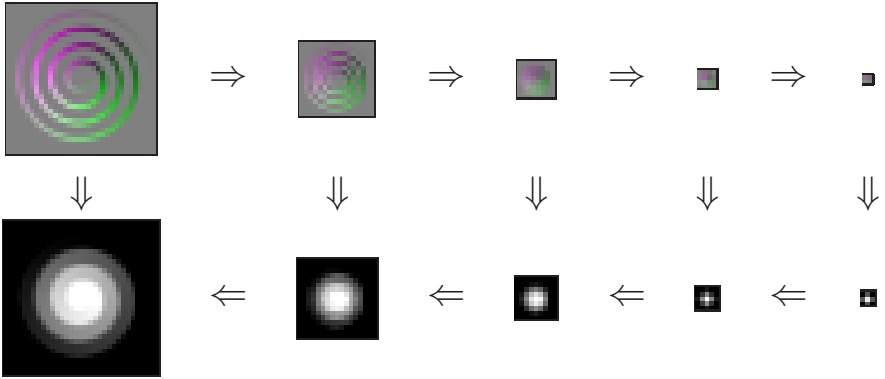


Figure 2: The multiscale integration method.

#### 3.1 The algorithm

The central part of our algorithm is the recursive procedure *ComputeHeights* below:

---

*ComputeHeights*( $f, g, w$ )

1. If  $f$  is small enough then
  2.  $z \leftarrow (0, 0, \dots, 0)$ ;
  3. else
  4.  $f' \leftarrow \text{ShrinkSlopes}(f, w)$ ;  $g' \leftarrow \text{ShrinkSlopes}(g, w)$ ;
  5.  $w' \leftarrow \text{ShrinkWeights}(w)$ ;
  6.  $z' \leftarrow \text{ComputeHeights}(f', g', w')$ ;
  7.  $z \leftarrow \text{ExpandHeights}(z')$ ;
  8.  $A, b \leftarrow \text{BuildSystem}(f, g, w)$ ;
  9.  $z \leftarrow \text{SolveSystem}(A, b, z)$ ;
  10. Return  $z$ .
- 

Note that our scheme differs substantially from the “pyramid-based” method of Chen, Wang and Wang [6]. For one thing, at each scale  $k$  the Poisson system of our method has  $N/4^k$  unknowns, instead of  $N$  as in their method.

**Inputs:** The the slope maps  $f, g$  and the weight map  $w$  should be three real-valued arrays with the same dimensions. Each sample  $f[u, v]$  is assumed to be an average of  $\partial Z / \partial x$  around the *slope sampling point*  $p[u, v] = (u + 1/2, v + 1/2)$ ; and similarly for  $g[u, v]$ . Each weight  $w[u, v]$  should be a non-negative number reflecting the relative trustworthiness of the corresponding slope values  $f[u, v], g[u, v]$ . The weight  $w[u, v]$  should be zero if the corresponding slopes are completely unreliable — in particular, if there may be a cliff crossing the pixel centered at  $p[u, v]$ . In that case, the data  $f[u, v]$  and  $g[u, v]$  will be completely ignored. Our algorithm assumes that  $w[u, v] = 0$  also for any pixels that lie outside the domain  $D$ .

**Outputs:** The algorithm returns an array of height samples  $z[u, v]$ , nominally taken at *height sampling points*  $q[u, v] = (u, v)$ , displaced from the slope sampling points  $p[u, v]$  by half a step in each direction. Because of these assumptions, the  $z$  array computed by our method will have one more column and one more row than the slope maps.

**Building the system:** Like other Poisson-based methods [17, 25], our algorithm builds in step 8 a linear equation system with one equation and one unknown for each height value  $z[u, v]$ . Each equation states the equality between two estimates of Laplacian  $\mathbf{L}(z) = \nabla \cdot (\nabla Z)$  at the point  $q[u, v]$ : one computed from the unknown heights (the left-hand side), and one from the given slope values (the right-hand side).

The precise nature of the estimates is not critical; our multiscale iterative method can be used with other Laplacian estimators, including non-linear ones. In our implementation [29], we use the equation  $-\mathcal{L}(z)[u, v] = -\mathcal{D}(f, g)[u, v]$ , where

$$-\mathcal{L}(z)[u, v] = z[u, v] - \frac{w_{-0}}{w_{00}}z_{-0} - \frac{w_{+0}}{w_{00}}z_{+0} - \frac{w_{0-}}{w_{00}}z_{0-} - \frac{w_{0+}}{w_{00}}z_{0+} \quad (1)$$

$$\begin{aligned} -\mathcal{D}(f, g) &= \frac{w_{--}}{w_{00}}f_{--} + \frac{w_{-+}}{w_{00}}f_{-+} - \frac{w_{+-}}{w_{00}}f_{+-} - \frac{w_{++}}{w_{00}}f_{++} \\ &+ \frac{w_{--}}{w_{00}}g_{--} + \frac{w_{+-}}{w_{00}}g_{+-} - \frac{w_{-+}}{w_{00}}g_{-+} - \frac{w_{++}}{w_{00}}g_{++} \end{aligned} \quad (2)$$

and, for all  $r, s \in \{-, +\} = \{-1, +1\}$ ,

$$\begin{aligned} f_{rs} &= f[u + r, v + s] & g_{rs} &= g[u + r, v + s] & w_{rs} &= w[u + r, v + s] \\ w_{0s} &= w_{+s} + w_{-s} & w_{r0} &= w_{r+} + w_{r-} \\ w_{00} &= w_{0+} + w_{0-} + w_{-0} + w_{+0} \\ z_{0s} &= z[u, v + s] & z_{r0} &= z[u + r, v] \end{aligned} \quad (3)$$

**Boundary cases:** These formulas assume that the weight  $w[u, v]$  is 0 if the corresponding point lies outside the domain  $D$ . With this convention, equation (3.1) can be used even along the margins of the domain  $D$ , or at grid corners  $q[u, v]$  that are adjacent to missing slope data. As long as one of the slope samples surrounding a point  $q[u, v]$  has nonzero weight, equation is valid and can be used to compute  $z[u, v]$  from its neighbors. As a consequence, the algorithm will patch up isolated one- to three-pixel “holes” in the data by integrating around them.

**Indeterminate values:** On the other hand, when all four slope values surrounding a pixel are missing the value of  $z[u, v]$  is essentially indeterminate. One may exclude those height values from the linear system, and set them to 0, NAN, or any other arbitrary value.

**Analysis:** To analyse the efficiency of this algorithm, we should consider what the steps do in the Fourier domain. When the slope maps are reduced, the higher-frequency components of the data are lost, while the remaining lower-frequency components have their wavelengths

reduced by one half. Therefore, the recursively computed solution  $z^{(k+1)}$  to the reduced problem, after being expanded to the original scale, will be mostly correct in the lower frequencies; only the small detail (at the scale of one or two pixels) will be missing. These details will be fixed by the Gauss-Seidel solver after a small number of iterations, largely independent of  $N$ . So, the recursive process is fast because each Fourier component of the height map gets computed at the scale where its wavelength is only a few pixels. Therefore, the time spent at scale  $k$  will be proportional  $N/4^k$ ; and the total time for all scales will be  $(1 + 1/4 + 1/4^2 + \dots + 1/4^m)O(N) < (4/3)O(N) = O(N)$ .

## 4 Robustness and accuracy

To test the robustness and accuracy of our method, we compared its output with that of representative implementations of the main competing methods.

**Data sets:** We used the slope datasets and weigh maps shown in figure 3. The sets `sbabel`, `spdome`, and `cbramp` were derived from mathematically defined height fields  $Z(x, y)$ . The `sbabel` field is  $C_1$ -smooth except at the ends of the ramp, with steep but not vertical walls. The `spdome` field has a slope discontinuity around the dome’s rim. The `cbramp` field is  $C_1$ -smooth along the ramp but has vertical cliffs on three sides. The gradient maps were obtained by Hann-weighted subsampling of the analytic derivatives, a process that results in some sampling noise at gradient discontinuities, and is completely oblivious to cliffs. In particular, the the cliffs around the top platform of `cbramp` are completely invisible in its slope map, and their location is defined only by the zeros in the given weight map. The `psface` data set is the gradient field of a human face, obtained by photometric stereo with the UWE MVL Photoface setup [10]. Its binary weight mask, created by hand with an image editor, excludes regions where the data is known to be unreliable.

**Methods:** Each dataset was processed with the algorithms listed in table 1. Methods AS, EM, ME, AT, UP were described by Agrawal *et. al* in 2006 [3]; we used their Matlab implementations [1], adapted to use our input and output file formats. Methods AS, EM, ME, AT use the weighted Poisson-based approach, with Matlab’s sparse matrix solver; the first three use iterative weight adjustment. However in AS and EM the weight map is internal and is neither accepted nor returned by the code. UP is an unweighted Poisson method whose linear system is solved by discrete cosine transform.

Table 1: Methods used in the accuracy tests. The third column tells whether the method accepts an external weight map.

Code	Type	$w$ input	Description
FC	Fourier transf.	No	Frankot-Chellappa [8, 15]
UP	Fourier transf.	No	Least Squares (unweighted Poisson) [1, 3]
AS	Direct sol.	No	$\alpha$ -Surface [3]
EM	Direct sol.	No	Energy Minimization [1, 3]
AT	Direct sol.	Yes	Affine Transforms (or Diffusion) [1, 3]
ME	Direct sol.	Yes	M-Estimators [1, 3]
MS	Multi-scale iter.	Yes	Our multiscale integration method [29]

**Reference solutions:** We compared the output of each method to that of Agrawal’s M-Estimators (ME) method, which appears to be the most accurate and robust of the lot. In

276 each case we computed the RMS error  $e$  between the two integrated height fields, after  
 277 shifting both to have zero mean; and the relative RMS error  $e/R$ , where  $R$  is the RMS value  
 278 of the two height fields. In these computations we considered only the parts of the domain  
 279 where the weight field  $w$  was nonzero.

280

281

282

283

284

285

286

287

288

289

290

291

292

293

294

295

296

297

298

299

300

301

302

303

304

305

306

307

308

309

310

311

312

313

314

315

316

317

318

319

320

321

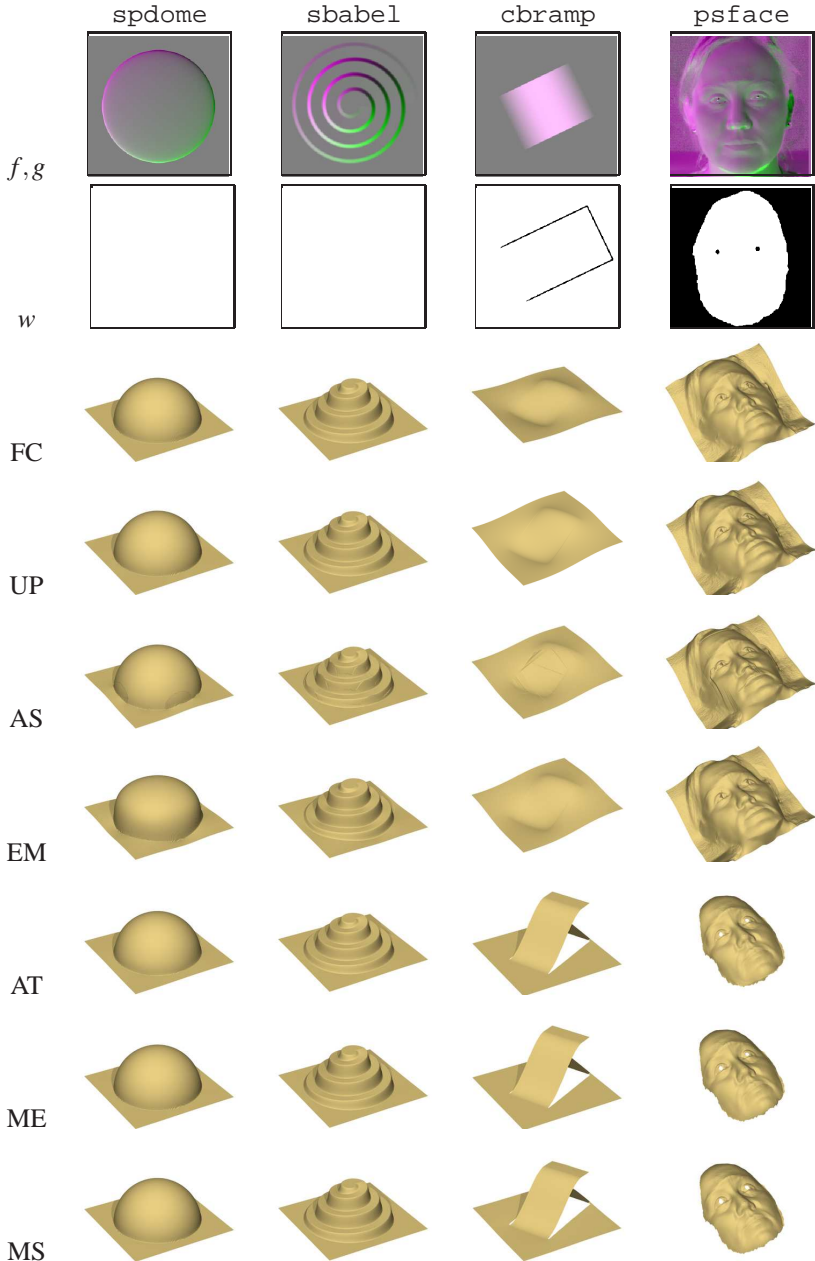


Figure 3: Datasets used in the tests, showing (from top to bottom) the gradient map  $f, g$ , the reliability weight map  $w$ , and the height field integrated by each method.

**Results and conclusions:** As table 2 and figure 3 show, the only methods that obtained usable results in all data sets were Agrawal’s Affine Transforms (AT) and M-Estimators (ME) methods, and our multiscale method (MS). The unweighted methods (FC and UP) and those which do not accept external weight maps (AS and EM) failed completely on the datasets with cliffs and invalid data.

Table 2: Relative RMS errors of each method from the ME reference solution.

Meth.	spdome		sbabel		cbramp		psface	
	$e$	$e/R$	$e$	$e/R$	$e$	$e/R$	$e$	$e/R$
FC	0.66	1.9%	0.56	2.1%	29.99	120.1%	19.47	98.0%
UP	0.14	0.4%	0.00	0.0%	29.61	107.1%	28.94	114.6%
AS	2.28	6.6%	3.22	12.5%	29.30	107.7%	29.76	106.0%
EM	4.82	13.4%	2.14	8.0%	29.61	107.0%	24.67	108.7%
AT	1.77	5.1%	3.17	12.3%	0.00	0.0%	0.10	0.7%
ME	0.00	0.0%	0.00	0.0%	0.00	0.0%	0.00	0.0%
MS	0.67	1.9%	0.60	2.2%	4.23	13.0%	0.73	3.9%

**Limitations** The multiscale approach is not valid in situations like figure 4, when the actual domain (the region where the weights are nonzero) includes a long and narrow corridor. After a couple of reductions, the corridor will be overrun by zero weights. Then the recursive solution will be useless as a starting guess, and the Gauss-Seidel iteration may take thousands iterations to converge. In such cases, direct solution of the linear system may be much faster than our method. How to make MS work in such cases is beyond the scope of this paper.

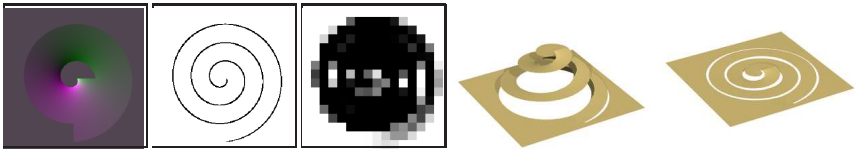


Figure 4: A pathological case for multiscale integration. From left to right:  $f^{(0)}$  and  $w^{(0)}$  ( $256 \times 256$ ),  $w^{(4)}$  ( $16 \times 16$ ), and the heights  $z$  obtained by ME and by our algorithm with 200 iterations per level.

## 5 Time and memory

**Datasets and methods:** To evaluate the efficiency of our method, we measured the computing time and memory needed for the integration of two square gradient fields, *spdome* and *psface*, sampled with various grid sizes from  $64 \times 64$  to  $512 \times 512$ .

We compared our method against two weighted Poisson integrators provided by Agrawal *et al.* [1], namely the Affine Transforms method (AT) and the weighted Poisson system builder and solver (PC) that is the innermost loop of their M-Estimator, Energy Minimisation, and  $\alpha$ -Surface methods. We removed the outermost loop of these last three methods since we are concerned only with the integration problem, not the problem of inferring the weight map. Those are the only methods in the literature that accept a reliability weight map (thus solving the same problem as ours) and are fast enough for practical use.

**Results and conclusions:** The results of these tests are shown in figure 5. The absolute running times are not directly comparable since our code is written in C and tuned to this task, while the other methods are implemented in Matlab using its built-in general-purpose sparse matrix functions. However, the plots in figure 5 (top) show that the running times scale quite differently: like  $O(N)$  for our algorithm (solid line). and apparently like  $O(N^{1.5})$  for the direct Poisson solvers (dashed lines).

Our multiscale integrator also uses less memory than the direct solvers; see figure 5 (bottom). Its memory usage is dominated by the Poisson system's matrix  $A$  which has at most  $5N$  nonzero entries and is stored in a specialized sparse data structure that uses  $60N$  bytes. The reduced-scale slope and weight maps use an additional  $5N$  bytes in all. The direct solving methods need to store the matrix  $A$  and also its upper triangular Gauss factor  $U$  (or, if  $A$  is symmetric, its Cholesky factor  $R$ ). For these methods, we counted the nonzero entries  $N_A$  in  $A$  and  $N_U$  in  $U$ , and estimated the memory usage as  $12N_A + 16N_U$  bytes assuming a general sparse matrix representation for  $U$ . We observed that  $N_A$  does not exceed  $5N$  for PC and  $7N$  for AT, but  $N_U$  is much larger and seems to grow like  $O(N^{1.15})$ . (dashed lines).

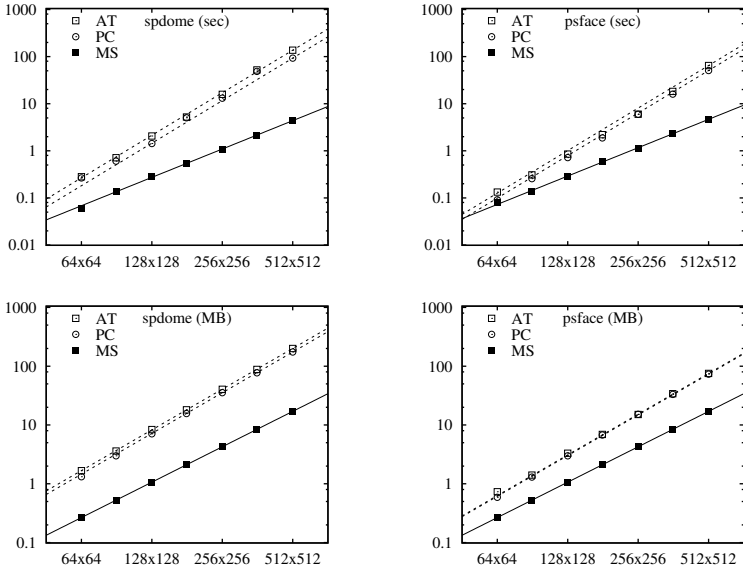


Figure 5: Top: Running time of two direct solving methods (PC,AT) and of our multiscale method (MS), in seconds. Bottom: Memory usage for the system's matrix  $A$  and its  $U$  factor (if any), in megabytes.

## 6 Conclusions

Our weighted multiscale integration algorithm is substantially faster and uses substantially less memory than other methods with comparable accuracy and robustness, both in practice and asymptotically. As far as we know, it is the only method that can integrate slope maps with missing data and cliffs of unknown height at megapixel resolution.

Our algorithm can be used on its own, with a given weight mask, or as the core of other methods that attempt to deduce the weight mask from the slope data and other clues. It can also be adapted to use other estimators for the Laplacian and divergent.

## References

- [1] A. Agrawal. Matlab/Octave code for robust surface reconstruction from 2d gradient fields. Available from <http://www.umiacs.umd.edu/~aagrawal/software.html>. Accessed on 2010-05-01, 2006. See [3].
- [2] A. Agrawal, R. Chellappa, and R. Raskar. An algebraic approach to surface reconstruction from gradient fields. In *Proc. 2005 Intl. Conf. on Computer Vision (ICCV)*, pages 174–181, 2005.
- [3] A. Agrawal, R. Raskar, and R. Chellappa. What is the range of surface reconstructions from a gradient field? In *Proc. 9th European Conf. on Computer Vision (ECCV)*, volume 3951, pages 578–591, 2006.
- [4] G. A. Atkinson and E. R. Hancock. Surface reconstruction using polarization and photometric stereo. In *Proc. 12th Intl. Conf. on Computer Analysis of Images and Patterns (CAIP)*, volume 4673, pages 466–473, 2007.
- [5] M. Chandraker, S. Agarwal, and D. Kriegman. ShadowCuts: Photometric stereo with shadows. In *CVPR07*, pages 1–8, 2007.
- [6] Y. Chen, H. Wang, and Y. Wang. Pyramid surface reconstruction from normal. In *Proc. 3rd IEEE Intl. Conf. on Image and Graphics (ICIG)*, pages 464–467, 2004.
- [7] R. Fraile and E. R. Hancock. Combinatorial surface integration. In *Proc. 18th Intl. Conf. on Pattern Recognition (ICPR'06) Volume 1*, pages 59–62, 2006.
- [8] R. T. Frankot and R. Chellappa. A method for enforcing integrability in shape from shading algorithms. *IEEE Trans. Pattern Analysis and Machine Intelligence*, 10(4): 439–451, 1988.
- [9] A. S. Georghiades, P. N. Belhumeur, and D. J. Kriegman. From few to many: Illumination cone models for face recognition under variable lighting and pose. *IEEE Transactions on Pattern Analysis and Machine Intelligence*, 23:643–660, 2001.
- [10] M. F. Hansen, G. A. Atkinson, L. N. Smith, and M. L. Smith. 3d face reconstructions from photometric stereo using near infrared and visible light. *Computer Vision and Image Understanding*, In Press, 2010. doi: 10.1016/j.cviu.2010.03.001.
- [11] B. K. P. Horn. Height and gradient from shading. *Intl. Journal of Computer Vision*, 5(1):37–75, 1990.
- [12] B. K. P. Horn and Michael J. Brooks. *Shape from Shading*. MIT Press, Cambridge, Mass., 1989.
- [13] B. K. P. Horn, R. J. Woodham, and W. M. Silver. Determining shape and reflectance using multiple images. Technical Report AI Memo 490, MIT Artificial Intelligence Laboratory, 1978.

- [14] M. Kampel and R. Sablatnig. 3D puzzling of archeological fragments. In Danijel Skocaj, editor, *Proc. of 9th Computer Vision Winter Workshop*, pages 31–40, 2004.
- [15] P. D. Kovesi. frankotchellappa.m: The Frankot-Chellappa gradient integrator in MATLAB/Octave. Univ. of Western Australia, <http://www.csse.uwa.edu.au/~pk/Research/MatlabFns/Shapelet/>, 2000.
- [16] H. C. G. Leitão, R. F. V. Saracchini, and J. Stolfi. Matching photometric observation vectors with shadows and variable albedo. In *Proc. 21th Brazilian Symp. on Computer Graphics and Image Processing (SIBGRAPI)*, pages 179–186, 2008.
- [17] B. K. P.Horn. Height and gradient from shading. Technical Report AI Memo 1105, Massachusetts Institute of Technology, 1989.
- [18] D. Reddy, A. Agrawal, and R. Chellappa. Enforcing integrability by error correction using  $\ell_1$ -minimization. In *Proc. 2009 IEEE Conf. on Computer Vision and Pattern Recognition*, pages 2350–2357, 2009.
- [19] A. Robles-Kelly and E. R. Hancock. Surface height recovery from surface normals using manifold embedding. In *Proc. Intl. Conf. on Image Processing (ICIP)*, 2004.
- [20] R. F. V. Saracchini, J. Stolfi, and H. C. G. Leitão. Shape reconstruction using a gauge-based photometric stereo method. In *Proceedings of CLEI*, 2009.
- [21] G. D. J. Smith and A. G. Bors. Height estimation from vector fields of surface normals. In *Proc. IEEE Intl. Conf. on Digital Signal Processing (DSP)*, pages 1031–1034, 2002.
- [22] J. Sun, M. L. Smith, L. N. Smith, S. Midha, and J. Bamber. Object surface recovery using a multi-light photometric stereo technique for non-Lambertian surfaces subject to shadows and specularities. *Image and Vision Computing*, 25(7):1050–1057, 2007.
- [23] J. Sun, M. L. Smith, L. N. Smith, L. Coutts, R. Dabis, C. Harland, and J. Bamber. Reflectance of human skin using colour photometric stereo - with particular application to pigmented lesion analysis. *Skin Research and Technology*, 14:173–179, 2008.
- [24] J. Sun, M. L. Smith, A. R. Farooq, and L. N. Smith. Concealed object perception and recognition using a photometric stereo strategy. In *Proc. 11th Intl. Conf. on Advanced Concepts for Intelligent Vision Systems (ACIVS)*, volume 5807, pages 445–455, 2009.
- [25] D. Terzopoulos. The computation of visible-surface representations. *IEEE Transactions on Pattern Analysis and Machine Intelligence*, 10(4):417–438, 1988.
- [26] T. Wei and R. Klette. Height from gradient using surface curvature and area constraints. In *Proc. 3rd Indian Conf. on Computer Vision, Graphics and Image Processing*, 2002.
- [27] R. J. Woodham. Photometric method for determining surface orientation from multiple images. *Optical Engineering*, 19(1):139–144, 1980.
- [28] Z. Wu and L. Li. A line-integration based method for depth recovery from surface normals. *Computer Vision, Graphics and Image Processing*, 43(1):53–66, 1988.
- [29] XXX. Xxx. Technical Report XXX, XXX, 2010.